اونيۏرسيتي مليسيا ڤهڠ
UNIVERSITI MALAYSIA PAHANG

ORIGINAL ARTICLE

Heat and mass transfer in non-coaxial rotation of radiative MHD Casson carbon nanofluid flow past a porous medium

W.N.N. Noranuar[1], A.Q. Mohamad[1,*], S. Shafie[1], I. Khan[2] and L.Y. Jiann[1]

[1] Department of Mathematical Sciences, Faculty of Science, Universiti Teknologi Malaysia, 81310 Johor Bahru, Johor, Malaysia.
[2] Basic Engineering Sciences Department, College of Engineering Majmaah University, Majmaah 11952, Saudi Arabia.

ABSTRACT – The heat and mass transfer of a radiative Casson nanofluid with single-wall and multi-wall carbon nanotubes in a non-coaxial rotating frame is analyzed in this article. The effects of thermal radiation, magnetic field and porosity are considered. Casson human blood is used to suspend both types of carbon nanotubes. The governed dimensional momentum, energy and concentration equations associated with initial and moving boundary conditions are converted into dimensionless expression by applying appropriate dimensionless variables. The exact solutions are determined by solving the dimensionless governing partial differential equations using the Laplace transform method. The obtained solutions are verified by comparing the present results with the published results. The validity of the solutions is assured since a precise agreement between the results is accomplished. The variation of the skin friction, Nusselt number, and Sherwood number for various values of the embedded parameters are presented in tables. The impacts of embedded parameters on the velocity, temperature and concentration profiles are illustrated in graphs. The distribution of the velocity and temperature is enhanced by the nanoparticles volume fraction but a reverse effect is observed for concentration profile. The radiation parameter has amplified the velocity and temperature of the Casson nanofluid. The emergence of porosity effect has aided to the smoothness of fluid flow but the presence of magnetic field reports the opposite effect on the velocity.

INTRODUCTION

The concept of rotating flow has been adapted in many applications of engineering and science including centrifugal pump, turbo fan jet engine, compressor, pipes, vacuum cleaner and rotating machinery. Owing to these crucial applications, the amount of research subjected to this topic has increased. The flow features and heat transportation for a rotating moving disk were investigated by Turkyilmazoglu [1] and Mohamad et al. [2]. In many geophysical and industry applications, the characteristics of the fluid flow are greatly affected by the Coriolis force and this leads to the formation of secondary flows [3]. The study of rotating flow for an incompressible fluid in porous medium and accelarated boundary can be found in [4, 5]. Interestingly, the flow can also be specifically rotated in a non-coaxial frame. Non-coaxial rotation is defined as the fluid flows that have two rotating axes which have been separated by a distance [6]. Mostly, the applications of this rotation can be found in engineering field such as the cooling devices with two fans, mixer machines with two kneaders, jet engines and cooling turbine blades [7]. Mohamad et al. [8] addressed the transportation of heat and mass for a non-coaxial rotating viscous fluid with time-dependent flow. The same work with double diffusion as [8] was also done by Mohamad et al. [9] for a second grade fluid and Mahanthesh et al. [10] for a Casson fluid. These studies [8-10] attained the exact solutions by using the Laplace transform method.

Magnetohydrodynamics (MHD) is known as the interaction of magnetic field in a moving electrical conducting fluid and this situation triggers the formation of Lorentz forces. The study of rotating fluid with MHD effect has grabbed many attention of the researchers in view of its great contribution in underground disposal of radioactive waste material, metal casting and liquid metal cooling blankets for fusion reactors, geothermal energy extractions and exothermic chemical reactions [11]. Guria [12] included MHD effect in investigating the viscous fluid flow in non-coaxial rotation with a periodic suction. Mohamad et al. [13] continued previous study [12] by addressing mass and heat transportation in a porous material. The study revealed that the velocity of the fluid has declined in response to the magnetic field. Mohamad et al. [14] presented similar outcome concerning the flow over accelerated non-coaxially rotating disk with the existence of MHD and porosity impacts. Noranuar et al. [15] continued the previous work [14] by considering double convective flow in a porous medium. The study observed that the porosity of the medium has enhanced the fluid velocity. Considering of the same type of rotation, Rana et al. [16] examined the consequences of chemical reaction and thermal radiation on the MHD flow via a porous medium with double diffusion. The study of fluid flow in a rotating frame incorporating with the impacts of MHD and porosity is also available in [17-19].

The effectiveness of the heat and mass transport processes, for example in heat exchangers and fuel cells are assured based on the type of fluid [20]. Fluid that disobey the Newton's Law of viscosity is called as the non-Newtonian fluid.

The study related to this type of fluid is limited due to the complexity of fluid behavior as compared to Newtonian fluid [21]. Besides, honey, ketchup, clay, mud, melted chocolate, paints, and egg whites are known as the materials that exhibit the non-Newtonian features with vary viscosity depend on the applied stress [22]. Casson fluid is classified as the non-Newtonian fluid and its rheological model is frequently used to describe the properties of human blood [23]. Several industries in science, engineering and medical field have adapted the Casson fluid model in their applications such as cancer therapy and fibrinogen, oil recovery system, building thermal insulation, and cooling sytem of electronic devices [24]. Recently, the development of nanofluid for several technologies has become a high demand due to its extensive applications in electronic, biomedical and industrial sector [25]. Theoretically, nanofluid is known as the colloidal mixture of two substances, the solid nano-sized particles (nanoparticles) and base fluid [26]. The role of nanofluid in performing heat transfer for a MHD rotating system with porosity by using classical nanoparticles such as Cu, Ag, Al, Al_2O^3 and TiO^3 had been carried out by Zin et al. [27] and Dinarvand and Pop [28]. Das et al. [29] had also used classical nanofluids to investigate MHD flow in a non-coaxial rotating system and embedded a porous disk. While Ashlin and Mahanthesh [30] used hybrid nanofluid to examine the heat source and radiation impacts on the flow with same type of rotation. Interestingly, carbon nanotubes (CNTs) as the dispersing nanoparticles have received significant attention because their thermal conductivity is higher as compared to the classical nanoparticles [31]. Acharya et al. [32] and Mahanthesh et al. [33] studied the impacts of single-wall carbon nanotubes (SWCNTs) and multi-wall carbon nanotubes (MWCNTs) on the MHD rotating flow over a stretching surface. The previous work is extended by Shah et al. [34] including thermal radiation effect. Kumam et al. [35] studied the motion of fluid in a rotating channel with radiative and MHD consequences by using the suspension CNTs in Casson base fluid. Other references on the flow features of using CNTs nanofluid with several effects are found in [36-38].

Based on the above literature, it can be seen that the MHD flow in a non-coaxial rotation with porosity effect for Casson nanofluid by using CNTs as the nanoparticles has not been discussed in any study. Inspired from the above study, the current study is to investigate the MHD Casson nanofluid flow in a porous medium induced by natural convection and non-coaxial rotation of moving disk with heat and mass transfer. The effects of thermal radiation, porosity and magnetic field are taken into account. The exact solutions of the dimensionless governing equations for the fluid problem are determined by using the Laplace transform method. Further analysis of the velocity, concentration and temperature fields under the influences of pertinent parameters is carried out by presenting the results in graphs and tables.

MATHEMATICAL FORMULATION OF THE PROBLEM

A non-coaxial rotation for an incompressible Casson nanofluid with heat and mass transfer is considered and the fluid flow is assumed to be time-dependent passing a vertical disk with an impulsive motion. The physical model for this problem is illustrated in Figure 1, where x and z are the Cartesian coordinates with x-axis is chosen as the upward direction and z-axis is the normal of it. The semi-finite space $z > 0$ is occupied by nanofluid that composed by constant kinematic viscosity v_{nf} of SWCNTs and MWCNTs suspended in human blood and acts as an electrically conducting fluid flowing through a porous medium. The disk is placed vertically along the x-axis with forward motion and a uniform transverse magnetic field of strength B_0 is applied orthogonal to it. The plane $x = 0$ is considered as rotation axes for both disk and fluid. Initially, at $t = 0$, the fluid and disk are retained at temperature T_∞ and concentration C_∞, and rotate about z'-axis with the same angular velocity Ω. After time $t > 0$, the fluid remains rotating at z'-axis while the disk begins to move with velocity U_0 and rotates at z-axis. Both rotations have a uniform angular velocity Ω. The temperature of the disk and concentration raises to T_w and C_w. The distance between the two axes of rotation is equal to ℓ. A radiative heat flux q_r is imposed along to flow direction, z −axis.
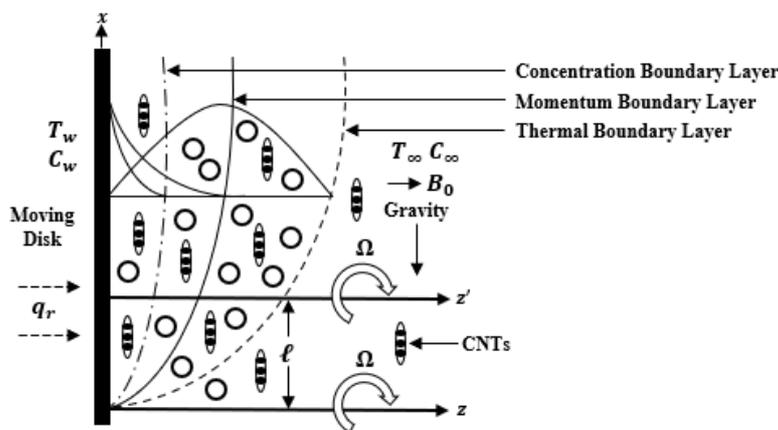
Figure 1. Physical geometry of the flow.

The governed dimensional partial differential equations (PDEs) corresponding to the above assumptions are given by

$$\rho_{nf}\frac{\partial F}{\partial t} + \left(\rho_{nf}\Omega i + \sigma_{nf}B_0{}^2 + \frac{\mu_{nf}}{k_1}\right) = \mu_{nf}\left(1 + \frac{1}{\gamma}\right)\frac{\partial^2 F}{\partial z^2} + \left(\rho_{nf}\Omega i + \sigma_{nf}B_0{}^2 + \frac{\mu_{nf}}{k_1}\right)\Omega\ell +$$

$$(\rho\beta_T)_{nf}g_x(T - T_\infty) + (\rho\beta_C)_{nf}g_x(C - C_\infty),$$

(1)

$$\left(\rho C_p\right)_{nf}\frac{\partial T}{\partial t} = k_{nf}\frac{\partial^2 T}{\partial z^2} - \frac{\partial q_r}{\partial z},$$

(2)

$$\frac{\partial C}{\partial t} = D_{nf}\frac{\partial^2 C}{\partial z^2}.$$

(3)

The following initial and boundary conditions are

$$F(z, 0) = \Omega\ell; \quad T(z, 0) = T_\infty; \quad C(z, 0) = C_\infty; \quad z > 0,$$

$$F(0, t) = U_0; \quad T(0, t) = T_w; \quad C(0, t) = C_w; \quad t > 0,$$

(4)

$$F(\infty, t) = \Omega\ell; \quad T(\infty, t) = T_\infty; \quad C(\infty, t) = C_\infty; \quad t > 0,$$

where $F = f + ig$ is the complex velocity with $f = f(z, t)$ is the primary velocity (real part) and $g = g(z, t)$ is the secondary velocity (imaginary part). Meanwhile, $\rho_{nf}, \sigma_{nf}, \mu_{nf}, (\beta_T)_{nf}, (\beta_C)_{nf}, \left(\rho C_p\right)_{nf}, k_{nf}$ and D_{nf} are the nanofluid constants for density, electrical conductivity, dynamic viscosity, thermal expansion coefficient, concentration expansion coefficient, heat capacitance, thermal conductivity and mass diffusivity, where all are clearly defined in Table 1. Besides, $\gamma = \mu_B\sqrt{2\pi_c}\Big/p_y$ is the Casson parameter and U_0 is the characteristic of velocity. After adopting Rosseland approximation, the radiative heat flux q_r in energy equation (2) is defined as

$$q_r = -\frac{4\sigma^*}{3k^*}\frac{\partial T^4}{\partial z}$$

(5)

Where k^* is the mean absorption coefficient and σ^* is the Stefan-Boltzmann constant. Then, the temperature difference between fluid temperature T and the free stream temperature T_∞ is assumed to be adequate small such that T^4 in equation (5) is a function of temperature which linearized by expanding into the Taylor Series about T_∞. Ignoring the higher order terms, it forms

$$T^4 \cong 4T_\infty{}^3 T - 3T_\infty{}^4.$$

(6)

Then, the substitution of equations (5) and (6) into equation (2) produces the following form of energy equation

$$\left(\rho C_p\right)_{nf}\frac{\partial T}{\partial t} = \left(k_{nf} + \frac{16\sigma^* T_\infty{}^3}{3k^*}\right)\frac{\partial^2 T}{\partial z^2}.$$

(7)

Thermophysical properties

In this study, the transmission of heat and flow features for both SWCNTs and MWCNTs are analyzed by substituting the nanofluid constant in equations (1), (3) and (7) with the properties presented in Table 1. These physical properties of nanofluid for CNTs are adopted from the theoretical model that has been introduced by Xue et al.[39].

Table 1. Physical properties of nanofluid.

Properties	Nanofluid
Density	$\rho_{nf} = (1 - \phi)\rho_f + \phi\rho_{CNTs}$
Electrical conductivity	$\dfrac{\sigma_{nf}}{\sigma_f} = 1 + \dfrac{3\left(\frac{\sigma_{CNTs}}{\sigma_f} - 1\right)\phi}{\left(\frac{\sigma_{CNTs}}{\sigma_f} + 2\right) - \phi\left(\frac{\sigma_{CNTs}}{\sigma_f} - 1\right)}$
Dynamic viscosity	$\mu_{nf} = \dfrac{\mu_f}{(1 - \phi)^{2.5}}$
Thermal expansion coefficient	$(\beta_T)_{nf} = \dfrac{(1 - \phi)(\rho\beta_T)_f + \phi(\rho\beta_T)_{CNTs}}{\rho_{nf}}$
Concentration expansion coefficient	$(\beta_C)_{nf} = \dfrac{(1 - \phi)(\rho\beta_C)_f + \phi(\rho\beta_C)_{CNTs}}{\rho_{nf}}$
Heat capacitance	$\left(\rho C_p\right)_{nf} = (1 - \phi)\left(\rho C_p\right)_f + \phi\left(\rho C_p\right)_{CNTs}$
Thermal conductivity	$\dfrac{k_{nf}}{k_f} = \dfrac{1 - \phi + 2\phi\frac{k_{CNTs}}{k_{CNTs} - k_f}ln\left(\frac{k_{CNTs} + k_f}{2k_f}\right)}{1 - \phi + 2\phi\frac{k_f}{k_{CNTs} - k_f}ln\left(\frac{k_{CNTs} + k_f}{2k_f}\right)}$
Mass diffusivity	$D_{nf} = (1 - \phi)D_f$

where ϕ is the solid volume fraction of nanofluid and the subscript f, nf and $CNTs$ denote for based fluid, nanofluid and carbon nanotubes, respectively. The above physical properties are then employed based on the thermophysical features in Table 2.

Table 2. Thermophysical features of human blood, SWCNTs and MWCNTs.

Materials \ Properties	Human Blood	SWCNTs	MWCNTs
$\rho(Kgm^{-1})$	1053	2600	1600
$C_p(JKg^{-1}K^{-1})$	3594	425	796
$k(Wm^{-1}K^{-1})$	0.492	6600	3000
$\beta \times 10^{-5}(K^{-1})$	0.8	27	44
$\sigma(Sm^{-1})$	0.18	$10^6 - 10^7$	1.9×10^{-4}

Dimensionless conversion

To transform the system of equations (1), (3), (7) and (4) into dimensionless forms, the following dimensionless variables as given by Mohamad et al. [13] are employed.

$$F^* = \frac{F}{\Omega\ell} - 1, \quad z^* = \sqrt{\frac{\Omega}{v}}z, \quad t^* = \Omega t, \quad T^* = \frac{T - T_\infty}{T_w - T_\infty}, \quad C^* = \frac{C - C_\infty}{C_w - C_\infty}. \tag{8}$$

Incorporating with the properties in Table 1, we have

$$\frac{\partial F}{\partial t} + d_1 F = \frac{1}{\phi_1}\left(1 + \frac{1}{\gamma}\right)\frac{\partial^2 F}{\partial z^2} + \phi_3 Gr T + \phi_3 Gm C, \tag{9}$$

$$\frac{\partial T}{\partial t} = \frac{1}{a_1}\frac{\partial^2 T}{\partial z^2}, \tag{10}$$

$$\frac{\partial C}{\partial t} = \frac{1}{a_2}\frac{\partial^2 C}{\partial z^2}, \tag{11}$$

associated with dimensionless conditions

$$F(z,0) = 0; \quad T(z,0) = 0; \quad C(z,0) = 0; \quad z > 0,$$

$$F(0,t) = U - 1; \quad T(0,t) = 1; \quad C(0,t) = 1; \quad t > 0, \tag{12}$$

$$F(\infty,t) = 0; \quad T(\infty,t) = 0; \quad C(\infty,t) = 0; \quad t > 0,$$

where

$$d_1 = \left(i + M^2\phi_2 + \frac{1}{\phi_1 K}\right), \quad a_1 = \frac{Pr\phi_4}{\lambda + Rd}, \quad a_2 = \frac{Sc}{(1-\phi)}, \quad Pr = \frac{\nu_f(\rho C_p)_f}{k_f}, \quad Sc = \frac{\nu_f}{D_f}, \quad M = \frac{\sigma_f B_0^{\,2}}{\Omega\rho_f},$$

$$\frac{1}{K} = \frac{\nu_f}{k_1\Omega}, \quad Gr = \frac{(\beta_T)_f g_x}{\Omega^2 \ell}(T_w - T_\infty), \quad Gm = \frac{(\beta_C)_f g_x}{\Omega^2 \ell}(C_w - C_\infty), \quad Rd = \frac{16\sigma^* T_\infty^{\,3}}{3k^* k_f}, \quad U = \frac{U_0}{\Omega\ell}.$$

Here, d_1, a_1 and a_2 are constant parameters, Pr is Prandtl number, Sc is Schmidt number, M is the magnetic field parameter, K is the porosity parameter, Gr is Grashof number, Gm is modified Grashof number, Rd is the radiation parameter and U is the amplitude of disk. The other constant parameters for the nanofluid are

$$\lambda = \frac{k_{nf}}{k_f}, \quad \phi_1 = (1-\phi)^{2.5}\left((1-\phi) + \frac{\phi\rho_{CNTs}}{\rho_f}\right),$$

$$\phi_2 = \left(1 + \frac{3\left(\frac{\sigma_{CNTs}}{\sigma_f} - 1\right)\phi}{\left(\frac{\sigma_{CNTs}}{\sigma_f} + 2\right) - \phi\left(\frac{\sigma_{CNTs}}{\sigma_f} - 1\right)}\right)\left((1-\phi) + \frac{\phi\rho_{CNTs}}{\rho_f}\right),$$

$$\phi_3 = \frac{(1-\phi) + \frac{\phi(\rho\beta)_{CNTs}}{(\rho\beta)_f}}{(1-\phi) + \frac{\phi\rho_{CNTs}}{\rho_f}}, \quad \phi_4 = (1-\phi) + \frac{\phi(\rho C_p)_{CNTs}}{(\rho C_p)_f}.$$

Exact solutions by laplace transform

To obtain the exact solutions for equations (9-12), the Laplace transform is used and subsequently produces the system in ordinary differential equations (ODEs) as

$$\frac{d^2}{dz^2}\bar{F}(z,q) - (n_1 q + n_2)\bar{F}(z,q) = -n_3 Gr\bar{T}(z,q) - n_3 Gm\bar{C}(z,q), \tag{13}$$

$$\frac{d^2}{dz^2}\bar{T}(z,q) - (a_1 q)\bar{T}(z,q) = 0, \tag{14}$$

$$\frac{d^2}{dz^2}\bar{C}(z,q) - (a_2 q)\bar{C}(z,q) = 0, \tag{15}$$

with the Laplace conditions

$$\bar{F}(0,q) = (U-1)\frac{1}{q}, \quad \bar{F}(\infty,q) = 0, \tag{16}$$

$$\bar{T}(0,q) = \frac{1}{q}, \quad \bar{T}(\infty,q) = 0, \tag{17}$$

$$\bar{C}(0,q) = \frac{1}{q}, \quad \bar{C}(\infty,q) = 0. \tag{18}$$

After that, the boundary conditions (16-18) are utilized to solve equations (13-15) and yields the following solutions in Laplace form.

$$\bar{F}(z,q) = \frac{U}{q}exp\left(-z\sqrt{n_1 q + n_2}\right) - \frac{1}{q}exp\left(-z\sqrt{n_1 q + n_2}\right) + \frac{n_3 Gr}{n_4 q(q-m_1)}exp\left(-z\sqrt{n_1 q + n_2}\right) +$$

$$\frac{n_3 Gm}{n_5 q(q-m_2)}exp\left(-z\sqrt{n_1 q + n_2}\right) - \frac{n_3 Gr}{n_4 q(q-m_1)}exp\left(-z\sqrt{a_1 q}\right) - \tag{19}$$

$$\frac{n_3 Gm}{n_5 q(q-m_2)}exp\left(-z\sqrt{a_2 q}\right),$$

$$\bar{T}(z,q) = \frac{1}{q}exp\left(-z\sqrt{a_1 q}\right), \tag{20}$$

$$\bar{C}(z,q) = \frac{1}{q}exp\left(-z\sqrt{a_2 q}\right). \tag{21}$$

After implemeting partial fraction on $n_3 Gr/n_4 q(q-m_2)$ and $n_3 Gr/n_5 q(q-m_3)$ as well as factorizing the term $\sqrt{n_1}$, equation (19) is simplified to

$$\bar{F}(z,q) = \frac{U}{q}exp\left(-z\sqrt{n_1}\sqrt{q+b_6}\right) - \frac{1}{q}exp\left(-z\sqrt{n_1}\sqrt{q+b_6}\right) - \frac{b_7}{q}exp\left(-z\sqrt{n_1}\sqrt{q+b_6}\right) +$$

$$\frac{b_7}{q-m_2}exp\left(-z\sqrt{n_1}\sqrt{q+b_6}\right) - \frac{b_8}{q}exp\left(-z\sqrt{n_1}\sqrt{q+b_6}\right) + \frac{b_8}{q-m_3}exp\left(-z\sqrt{n_1}\sqrt{q+b_6}\right) + \tag{22}$$

$$\frac{b_7}{q}exp\left(-z\sqrt{a_1 q}\right) - \frac{b_7}{q-m_2}exp\left(-z\sqrt{a_1 q}\right) + \frac{b_8}{q}exp\left(-z\sqrt{a_2 q}\right) - \frac{b_8}{q-m_3}exp\left(-z\sqrt{a_3 q}\right).$$

The solution for the governed problem are finally attained by imposing equations (20-21) and (22) with the inverse Laplace transform. Thus, it gives

$$F(z,t) = F_1(z,t) - F_2(z,t) - F_3(z,t) + F_4(z,t) - F_5(z,t) + F_6(z,t) + F_7(z,t) - F_8(z,t) +$$
$$F_9(z,t) - F_{10}(z,t), \tag{23}$$

$$T(z,t) = erfc\left(\frac{z}{2}\sqrt{\frac{a_1}{t}}\right), \tag{24}$$

$$C(z,t) = erfc\left(\frac{z}{2}\sqrt{\frac{a_2}{t}}\right), \tag{25}$$

with

$$F_1(z,t) = \frac{U}{2}\left[\exp(z\sqrt{n_1 b_6})erfc\left(\frac{z}{2}\sqrt{\frac{n_1}{t}} + \sqrt{b_6 t}\right) + \exp(-z\sqrt{n_1 b_6})erfc\left(\frac{z}{2}\sqrt{\frac{n_1}{t}} - \sqrt{b_6 t}\right)\right],$$

$$F_2(z,t) = \frac{1}{2}\left[\exp(z\sqrt{n_1 b_6})erfc\left(\frac{z}{2}\sqrt{\frac{n_1}{t}} + \sqrt{b_6 t}\right) + \exp(-z\sqrt{n_1 b_6})erfc\left(\frac{z}{2}\sqrt{\frac{n_1}{t}} - \sqrt{b_6 t}\right)\right],$$

$$F_3(z,t) = \frac{b_7}{2}\left[\exp(z\sqrt{n_1 b_6})erfc\left(\frac{z}{2}\sqrt{\frac{n_1}{t}} + \sqrt{b_6 t}\right) + \exp(-z\sqrt{n_1 b_6})erfc\left(\frac{z}{2}\sqrt{\frac{n_1}{t}} - \sqrt{b_6 t}\right)\right],$$

$$F_4(z,t) = \frac{b_7}{2}\left[\exp\left(m_1 t + z\sqrt{n_1(b_6 + m_1)}\right)erfc\left(\frac{z}{2}\sqrt{\frac{n_1}{t}} + \sqrt{(b_6 + m_1)t}\right)\right.$$
$$\left. + \exp\left(m_1 t - z\sqrt{n_1(b_6 + m_1)}\right)erfc\left(\frac{z}{2}\sqrt{\frac{n_1}{t}} - \sqrt{(b_6 + m_1)t}\right)\right],$$

$$F_5(z,t) = \frac{b_8}{2}\left[\exp(z\sqrt{n_1 b_6})erfc\left(\frac{z}{2}\sqrt{\frac{n_1}{t}} + \sqrt{b_6 t}\right) + \exp(-z\sqrt{n_1 b_6})erfc\left(\frac{z}{2}\sqrt{\frac{n_1}{t}} - \sqrt{b_6 t}\right)\right],$$

$$F_6(z,t) = \frac{b_8}{2}\left[\exp\left(m_2 t + z\sqrt{n_1(b_6 + m_2)}\right)erfc\left(\frac{z}{2}\sqrt{\frac{n_1}{t}} + \sqrt{(b_6 + m_2)t}\right)\right.$$
$$\left. + \exp\left(m_2 t - z\sqrt{n_1(b_6 + m_2)}\right)erfc\left(\frac{z}{2}\sqrt{\frac{n_1}{t}} - \sqrt{(b_6 + m_2)t}\right)\right],$$

$$F_7(z,t) = b_7\left[erfc\left(\frac{z}{2}\sqrt{\frac{a_1}{t}}\right)\right],$$

$$F_8(z,t) = \frac{b_7}{2}\left[\exp(m_1 t + z\sqrt{a_1 m_1})erfc\left(\frac{z}{2}\sqrt{\frac{a_1}{t}} + \sqrt{m_1 t}\right) + \exp(m_1 t - z\sqrt{a_1 m_1})erfc\left(\frac{z}{2}\sqrt{\frac{a_1}{t}} - \sqrt{m_1 t}\right)\right],$$

$$F_9(z,t) = b_8\left[erfc\left(\frac{z}{2}\sqrt{\frac{a_2}{t}}\right)\right],$$

$$F_{10}(z,t) = \frac{b_8}{2}\left[\exp(m_2 t + z\sqrt{a_1 m_2})erfc\left(\frac{z}{2}\sqrt{\frac{a_2}{t}} + \sqrt{m_2 t}\right) + \exp(m_2 t - z\sqrt{a_1 m_2})erfc\left(\frac{z}{2}\sqrt{\frac{a_2}{t}} - \sqrt{m_2 t}\right)\right],$$

where

$$b_6 = \frac{n_2}{n_1}, \quad b_7 = \frac{n_3 Gr}{n_4 m_1}, \quad b_8 = \frac{n_3 Gm}{n_5 m_2}, \quad n_0 = \frac{\gamma}{\gamma + 1}, \quad n_1 = \phi_1 n_0, \quad n_2 = d_1 n_1, \quad n_3 = \phi_3 n_1, \quad n_4 = a_1 - n_1,$$

$$n_5 = a_2 - n_1, \quad m_1 = \frac{n_2}{n_4}, \quad m_2 = \frac{n_2}{n_5}, \text{ are the constant parameters.}$$

Physical quantities

The dimensional skin friction, Nusselt number and Sherwood number for Casson nanofluid in non-coaxial rotation are defined as

$$\tau(t) = -\mu_{nf}\left(1 + \frac{1}{\gamma}\right)\frac{\partial F}{\partial z}\Big|_{z=0}, \tag{26}$$

$$Nu = -k_{nf}\frac{\partial T}{\partial z} + q_r\Big|_{z=0}, \tag{27}$$

$$Sh = -D_{nf}\frac{\partial C}{\partial z}\Big|_{z=0}. \tag{28}$$

Inserting related dimensionless variables (8) in equations (26-28) will reduce these equations to the dimensionless form as

$$\tau(t) = -\frac{1}{(1-\phi)^{2.5}}\left(1 + \frac{1}{\gamma}\right)\frac{\partial F}{\partial z}\Big|_{z=0}$$
$$= \tau_1(t) - \tau_2(t) - \tau_3(t) + \tau_4(t) - \tau_5(t) + \tau_6(t) + \tau_7(t) - \tau_8(t) + \tau_9(t) + \tau_{10}(t), \tag{29}$$

$$Nu = -\left(\frac{k_{nf}}{k_f} + Rd\right)\frac{\partial T}{\partial z}\Big|_{z=0} = (\lambda + Rd)\sqrt{\frac{a_1}{\pi t}}, \tag{30}$$

$$Sh = -(1-\phi)\frac{\partial C}{\partial z}\Big|_{z=0} = (1-\phi)\sqrt{\frac{a_2}{\pi t}}. \tag{31}$$

Solution validation

The validity of the obtained solutions for velocity is checked by comparing the current results with previously published analytical study by Mohamad et al. [7] which also applied the method of Laplace transform in their study. The comparison is conducted by letting $M = \phi = Sc = Gm = 0$, $K \to \infty$ and $\gamma \to \infty$ for the present results and the previous study at $\omega = 0$. The comparison indicates both the results are identical as illustrated in Figure 2. Furthermore, the numerical Gaver-Stehfest algorithm [40, 41] is also used to check the accuracy of present results where the values have satisfied with a slight difference and have been listed in Table 3 and 4. Satisfyingly, both comparisons come out with an excellent agreement and the validity is verified.
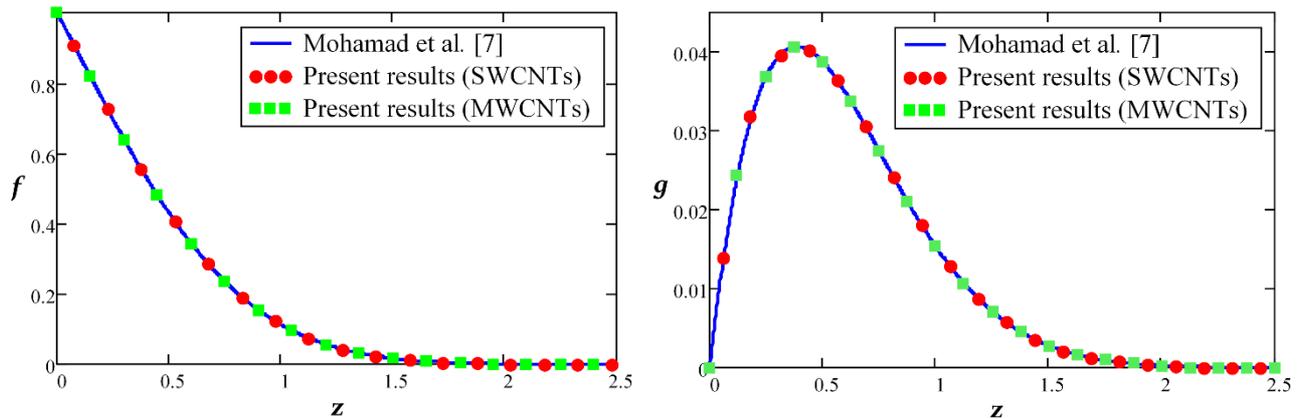
Figure 2. Verification present primary and secodary velocity results with the published results.

Table 3. Comparison of results by exact solution and numerical Gaver-Stehfest algorithm for primary velocity at $\gamma = Rd = 0.5, \phi = 0.02, Gr = Gm = 0.5, K = U = 2.0, M = t = 0.2, \Pr = 21$ and $Sc = 0.94$.

z	Primary velocity					
	SWCNTs			MWCNTs		
	Exact Equation 23	**Numerical** Equation 19	**Value error**	**Exact** Equation 23	**Numerical** Equation 19	**Value error**
0	1.0000	1.0000	0	1.0000	1.0000	0
0.5	0.7216	0.7217	0.0001	0.7257	0.7258	0.0001
1.0	0.4025	0.4027	0.0002	0.4079	0.4082	0.0003
1.5	0.1850	0.1851	0.0001	0.1895	0.1896	0.0001
2.0	0.0715	0.0716	0.0001	0.0743	0.0744	0.0001
2.5	0.0233	0.0234	0.0001	0.0246	0.0247	0.0001
3.0	0.0064	0.0064	0	0.0069	0.0069	0

Table 4. Comparison of results by exact solution and numerical Gaver-Stehfest algorithm for secondary velocity at $\gamma = Rd = 0.5, \phi = 0.02, Gr = Gm = 0.5, K = U = 2.0, M = t = 0.2, \Pr = 21$ and $Sc = 0.94$.

z	Secondary velocity					
	SWCNTs			MWCNTs		
	Exact Equation 23	**Numerical** Equation 19	**Value error**	**Exact** Equation 23	**Numerical** Equation 19	**Value error**
0	0.0000	0.0000	0	0.0000	0.0000	0
0.5	0.0399	0.0399	0	0.0398	0.0398	0
1.0	0.0368	0.0368	0	0.0370	0.0370	0
1.5	0.0218	0.0219	0.0001	0.0223	0.0223	0
2.0	0.0099	0.0099	0	0.0102	0.0102	0
2.5	0.0036	0.0036	0	0.0038	0.0038	0
3.0	0.0010	0.0010	0	0.0011	0.0011	0

RESULTS AND DISCUSSION

The non-coaxial rotating Casson nanofluid flow features with heat and mass diffusion in the view of several values of embedded parameters are illustrated in graphs by using MathCAD. Due to the rotating system, the velocity profiles are presented in complex variables, where the velocity are presented in two parts: primary velocity f and secondary velocity g. The existence of the Coriolis forces has affected the flow to be deflected, which leads to the formation of secondary velocity. The Casson nanofluid is composed by the SWCNTs and MWCNTs nanoparticles that has been suspended in human blood. Some graphs and tables are presented to display the impacts of Casson parameter γ, radiation parameter Rd, nanoparticle volume fraction ϕ, porosity parameter K, magnetic field M and time t. Default values of the involved parameters are considered as $\gamma = 0.5, Rd = 0.5, \phi = 0.02, M = 0.2, K = 2.0, t = 0.2$ unless otherwise prescribed. In this study, the effects of γ, K and M can been addressed in the velocity profiles only because these parameters have involved in the momentum equation. However, the presence of ϕ and t in all the governing equations has caused all profiles are under their influences.

Figure 3 illustrates the flow characteristics for varying values of γ. It is worth noting that the non-Newtonian behavior of Casson fluid is greatly influenced by the γ. As γ ascends, the primary and secondary velocities show decreasing trend due to increment of resistance in the flow. In other words, increasing γ is equivalent to the diminution of yield stress

which later reduces the fluid velocity. Moreover, when γ approaches infinity ($\gamma \to \infty$), the Casson problem reduces to a Newtonian problem. The consequences of Rd on the velocity and temperature distributions are exhibited in Figures 4 and 5. When Rd level is higher, the flow gets more heat energy and causes the growth in velocity and temperature profiles. Noting that, imposing intense Rd improves the energy mobility within the fluid, resulting an increase in the rate of heat transport. On the other hands, the heat energy supplied by Rd reduces fluid viscosity and subsequently drifts the velocity (primary and secondary).

Figures 6-8 depict the impacts of ϕ on velocity, temperature and concentration profiles. These figures reveal that the insertion of a high volume of nanoparticles causes to an elevation in the velocity (primary and secondary) profile and is accompanied by the thickening of the boundary layer. Besides, the temperature profile also shows an increasing trend in response to the ascend of ϕ. This effect is owing to enhancement of nanofluid's thermal conductivity due to increasing ϕ and significantly improves the heat conduction of the fluid. Therefore, the fluid becomes hotter. However, a contrast effect on concentration profile is noticed where a thinning of boundary layer and reduction profile are observed as ϕ is enhanced. Figure 9 shows the nature of velocity in response to M. The Lorentz forces which also known as the resistive type force in the fluid flow have improved as M has grown larger, and it functions as a flow retarder. Thus, the fluid velocity (primary and secondary) reduces as M increases.

Figure 10 presents the velocity propagation under the influence of K. The velocity (primary and secondary) profiles are observed to escalate when K is augmented. Noting that the effect of porosity K can also affect the permeablity of a medium, where higher K causes the medium to be more permeable and easily allows the fluid to flow. In other words, the fluid can effortlessly pass the medium with the aid of K. Next, the same effect of K is also observed for the impacts of t on the velocity, temperature and concentration profiles. Their behaviours are clearly illustrated in Figures 11-13. Higher velocity (primary and secondary), temperature and concentration profiles are achieved when larger t is imposed. When t increases, more thermal energy and mass are supplied to the flow. Therefore, the fluid become hotter and more concentrated.
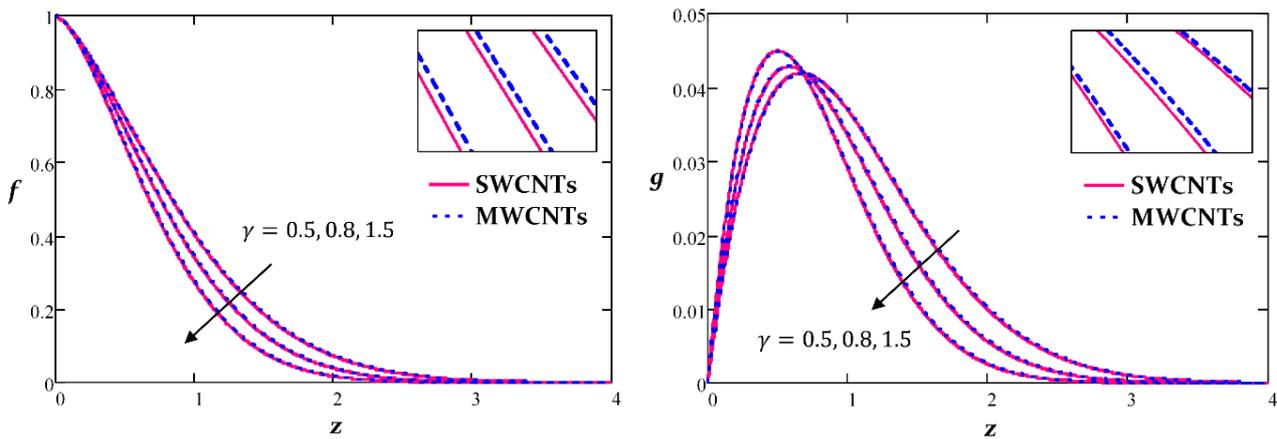
Figure 3. Influence of γ on f and g profiles.
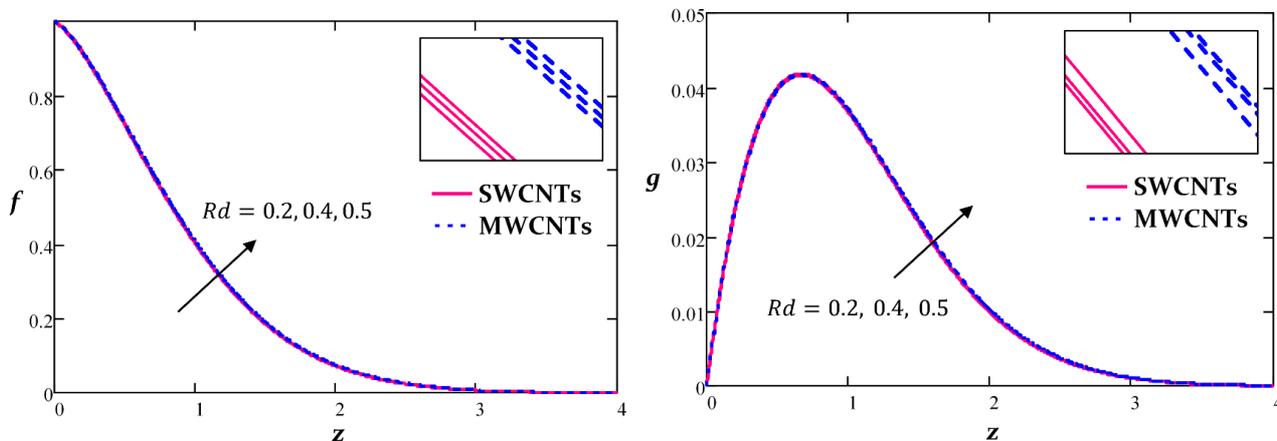
Figure 4. Influence of Rd on f and g profiles.
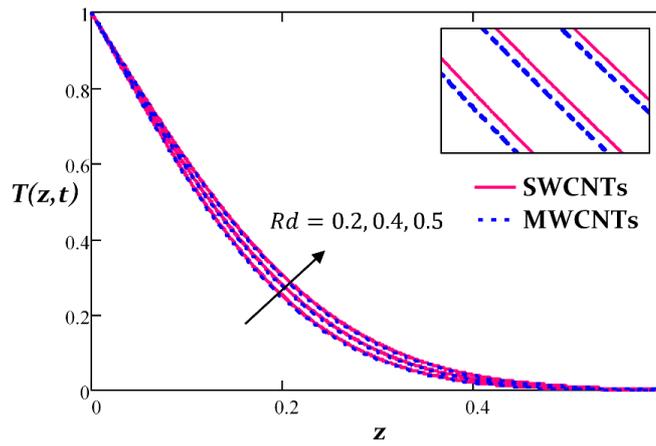
Figure 5. Influence of Rd on temperature profile.
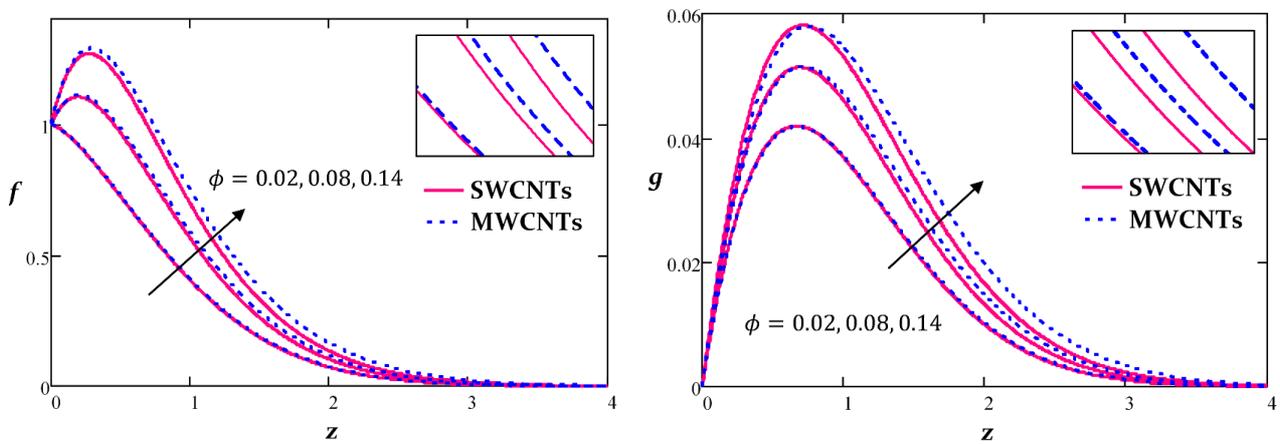
Figure 6. Influence of ϕ on f and g profiles.
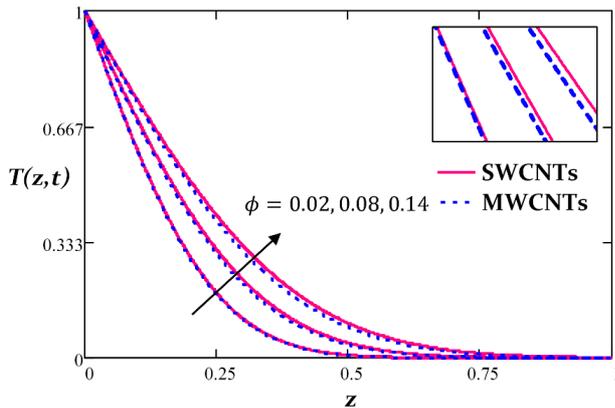
Figure 7. Influence of ϕ on temperature profile.
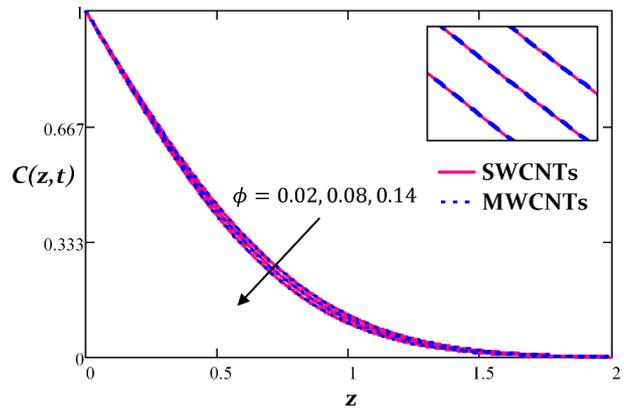
Figure 8. Influence of ϕ on concentration profile.

For the comparison between the effects of SWCNTs and MWCNTs, both types of CNTs have exhibited a similar nature on the velocity, temperature and concentration profiles. To be specific, in the case of velocity profiles, it suggests that MWCNTs have higher magnitude of velocity as compared to SWCNTs. This particular effect by MWCNTs is due to having lower density properties by which its suspension in human blood will result in a low-density nanofluid. For temperature profiles, it can be seen that the temperature of SWCNTs is higher than those of MWCNTs. This finding has been affected by the high thermal conductivity of SWCNTs and its immersion in human blood will produce a better heat conduction nanofluid. Based on temperature profiles, Figures 5, 7 and 12, since the wall temperature has been imposed, the fluid exhibits high temperature when the fluid is near to the disk. After that, the temperature gradually drops when the fluid aways from the surface. Meanwhile, based on Figures 8 and 13, both SWCNTs and MWCNTs have the same magnitude of concentration profiles because it shares the same value of mass diffusivity of nanofluid.

The results of the skin friction, Nusselt number and Sherwood number are listed in Tables 5-7, respectively. In Table 5, it is observed that the augment of Rd, ϕ, Gr, Gm, K and t decrease the skin friction (primary and secondary) for both SWCNTs and MWCNTs cases. This implies that less friction drag is produced between the fluid and surface which result in the enhancement of the velocity. However, the increase of M increases the skin friction (primary and secondary) for SWCNTs and MWCNTs cases. This is because when magnetic field becomes stronger, a large friction drag between the fluid and surface is produced and resists the fluid flow. Based on Table 6, suggests that the rate of heat transfer based on the results of Nu increases when Rd and ϕ are enhanced. Physically, the increase of ϕ has directly decreased the heat capacitance of nanofluid. Therefore, heat transportation occurs at a high rate. Likewise, for Sherwood number in Table 7, it reveals that the rate of mass transportation deteriorates as ϕ increases due to the decrease of mass transfer properties inside a fluid. Tables 6 and 7 observe that the rate of heat and mass transfer decrease in response to the ascend of t.
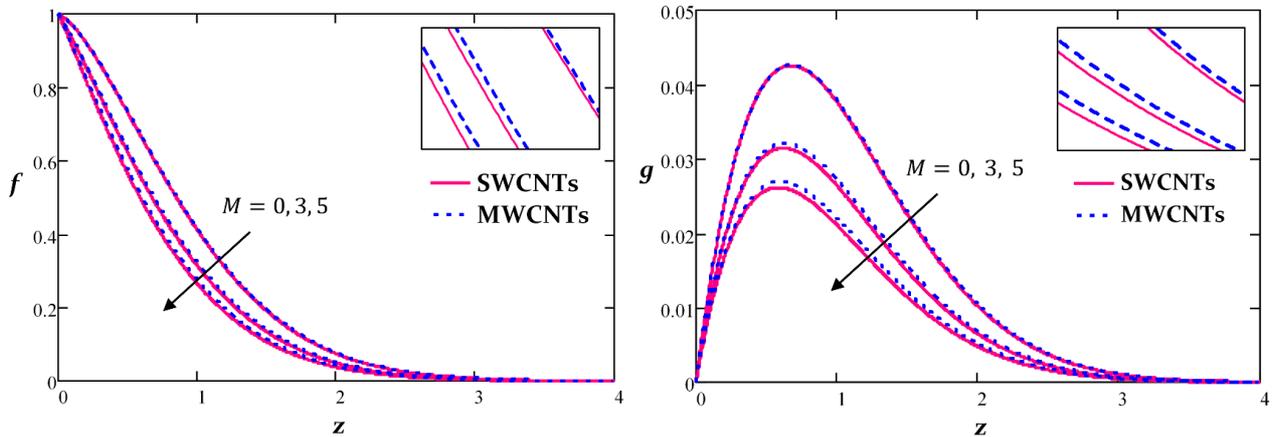
Figure 9. Influence of M on f and g profiles.
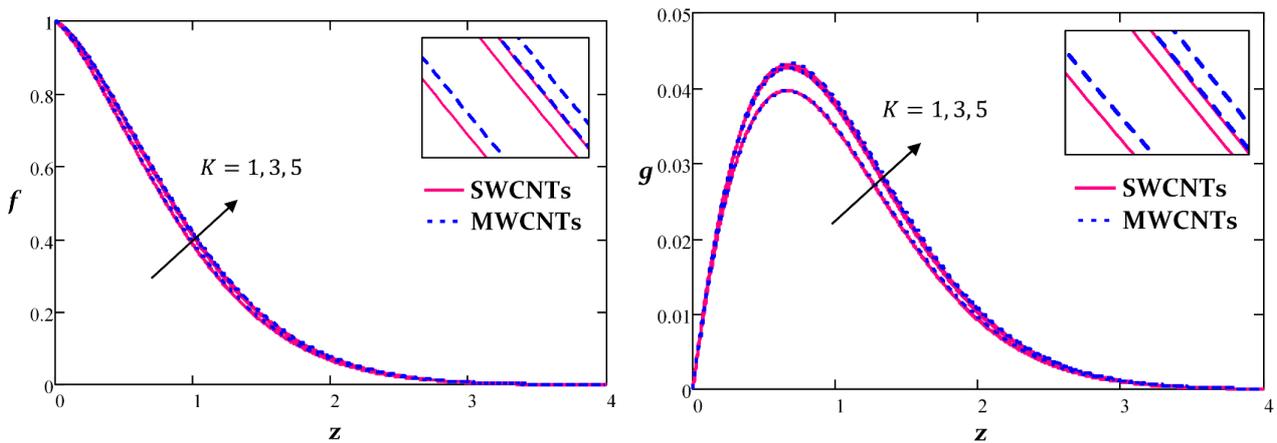
Figure 10. Influence of K on f and g profiles.
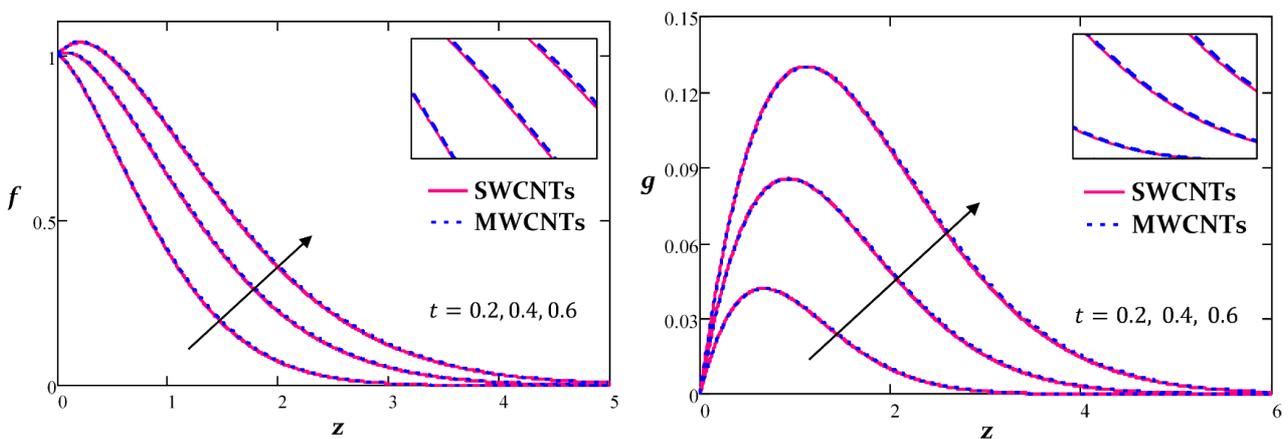
Figure 11. Influence of t on f and g profiles.
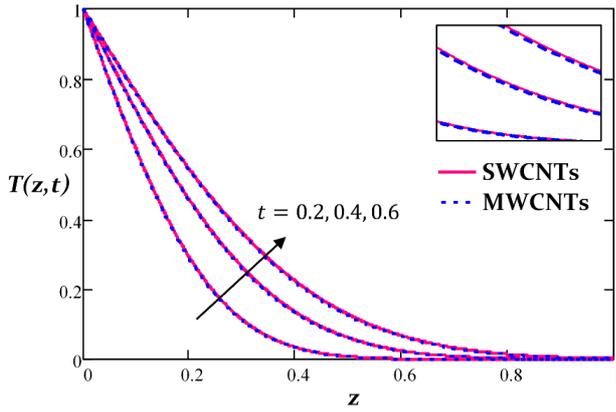
Figure 12. Influence of t on temperature profile.
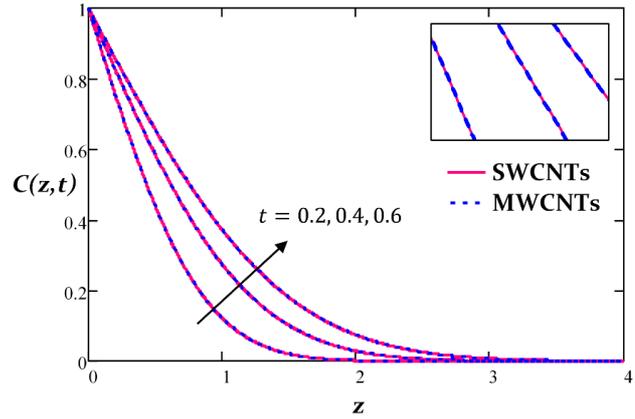
Figure 13. Influence of t on concentration profile.

Table 5. Variation of primary τ_p and secondary τ_s skin friction for SWCNTs and MWCNTs.

γ	Rd	ϕ	Gr	Gm	M	K	t	U	SWCNTs		MWCNTs	
									τ_p	τ_s	τ_p	τ_s
0.5	**0.2**	**0.02**	**0.5**	**0.5**	**0.2**	**2.0**	**0.2**	**2**	0.5249	-0.4830	0.5707	-0.4740
0.8	0.2	0.02	0.5	0.5	0.2	2.0	0.2	2	0.2889	-0.4256	0.3286	-0.4176
0.5	**0.4**	0.02	0.5	0.5	0.2	2.0	0.2	2	0.4984	-0.4835	0.5438	-0.4744
0.5	0.2	**0.08**	0.5	0.5	0.2	2.0	0.2	2	-4.9596	-0.6597	-5.0149	-0.6336
0.5	0.2	0.02	**5**	0.5	0.2	2.0	0.2	2	-3.9711	-0.5227	-3.8942	-0.5124
0.5	0.2	0.02	0.5	**5**	0.2	2.0	0.2	2	-13.0644	-0.8488	-13.0483	-0.8359
0.5	0.2	0.02	0.5	0.5	**3**	2.0	0.2	2	3.9996	-0.2997	1.7423	-0.4031
0.5	0.2	0.02	0.5	0.5	0.2	**3**	0.2	2	0.4424	-0.4884	0.4882	-0.4793
0.5	0.2	0.02	0.5	0.5	0.2	2.0	**0.4**	2	-0.8134	-0.7180	-0.7297	-0.6981
0.5	0.2	0.02	0.5	0.5	0.2	2.0	0.2	**3**	3.0593	-0.9210	3.1506	-0.9034

Table 6. Variation of Nusselt number Nu for SWCNTs and MWCNTs.

Rd	ϕ	t	Nu	
			SWCNTs	MWCNTs
0.2	**0.02**	**0.2**	7.1686	7.0974
0.4	0.02	0.2	7.6143	7.5478
0.2	**0.08**	0.2	9.2814	9.0623
0.2	0.02	**0.4**	5.0689	5.0186

Table 7. Variation of Sherwood number Sh for SWCNTs and MWCNTs.

ϕ	t	Sh	
		SWCNTs	MWCNTs
0.02	**0.2**	0.9991	0.9991
0.08	0.2	0.9680	0.9680
0.02	**0.4**	0.7065	0.7065

CONCLUSION

The present study has investigated the double diffusion in non-coaxial rotating frame for MHD radiative Casson nanofluid flow with a moving disk saturated in a porous medium. The investigation is carried out by considering human blood as the Casson base fluid and SWCNTs and MWCNTs as the dispersing nanoparticles. The problem has been analytically solved for the exact solutions of concentration, temperature and velocity profiles by using the Laplace transform method. Further analysis on the profiles affected by pertinent parameters are done by plotting the solutions graphically together with the comprehensive discussion. The following are some significant findings from the study which are

  i. The primary and secondary velocity profiles decline in response to the ascend of γ and M.
  ii. The primary and secondary velocity profiles escalate in response to the increase of Rd, ϕ, Gr, Gm, K and t.
  iii. Increment of Rd, ϕ and t enlarges the temperature profiles and thickening the thermal boundary layer.
  iv. The concentration profiles deteriorate with the increasing of ϕ values but it improves with the increasing t.
  v. MWCNTs has produced a prominent effect on the velocity (primary and secondary) profiles as compared to SWCNTs nanofluid.
  vi. For temperature profiles, prominent effect is exhibited by using SWCNTs because of their high thermal conductivity properties.
  vii. Decrement of skin friction are reported by the increasing of Rd, ϕ, Gr, Gm, K and t while opposite tendency is shown by M.
  viii. The rate of heat transportation increases proportionally to Rd and ϕ but a negative effect is shown by t.
  ix. The increase of ϕ and t has lowered the rate of mass transfer.

ACKNOWLEDGEMENT

REFERENCES

[1] T. Turkyilmazoglu, "Fluid flow and heat transfer over a rotating and vertically moving disk," Physics of Fluids., vol. 30, pp. 063605, 2018.

[2] A. Q. Mohamad, N. A. Jaafar, S. Shafie, Z. Ismail and M. Qasim, "Theoretical study on rotating casson fluid in moving channel disk," Journal of Physics: Conference Series., vol. 1366, no. 1, pp. 012039, 2019.

[3] S. Das, R. N. Jana and O. D. Makinde, "Transient hydromagnetic reactive Couette flow and heat transfer in a rotating frame of reference," Alexandria Engineering Journal., vol. 55, no. 1, pp. 635-644, 2016.

[4] M. V. Krishna, N. A. Ahamad and A. J. Chamkha, "Hall and ion slip effects on unsteady MHD free convective rotating flow through a saturated porous medium over an exponential accelerated plate," Alexandria Engineering Journal., vol. 59, no. 2, pp. 565-577, 2020.

[5] R. K. Deka, A. Paul and A. Chaliha, "Transient free convection flow past an accelerated vertical cylinder in a rotating fluid," Ain Shams Engineering Journal., vol. 5, no. 2, pp. 505-513, 2014.

[6] M. Guria, A. K. Kanch, S. Das and R. N. Jana, "Effects of Hall current and slip condition on unsteady flow of a viscous fluid due to non-coaxial rotation of a porous disk and a fluid at infinity," Meccanica., vol. 45, no. 1, pp. 23-32, 2010.

[7] A. Q. Mohamad, I. Khan, Z. Ismail and S. Shafie, "Exact solutions for unsteady free convection flow over an oscillating plate due to non-coaxial rotation," Springerplus., vol. 5, no. 1, pp. 1-22, 2016.

[8] A. Q. Mohamad, I. Khan, S. Shafie, Z. M. Isa and Z. Ismail, "Non-coaxial rotating flow of viscous fluid with heat and mass transfer," Neural Computing and Applications., vol. 30, no. 9, pp. 2759-2769, 2017.

[9] A. Q. Mohamad, L. Y. Jiann, I. Khan, N. A. M. Zin, S. Shafie and Z. Ismail, "Analytical solution for unsteady second grade fluid in presence of non-coaxial rotation," Journal of Physics: Conference Series., vol. 890, no. 012040, pp. 1-7, 2017.

[10] B. Mahanthesh, T. Brizlyn, S. A. Shehzad and B. J. Gireesha, "Nonlinear thermo-solutal convective flow of Casson fluid over an oscillating plate due to non-coaxial rotation with quadratic density fluctuation," Multidiscipline Modeling in Materials and Structures., vol. 15, no. 4, pp. 818-842, 2019.

[11] S. Das, B. Tarafdar and R. N. Jana, "Hall effects on unsteady MHD rotating flow past a periodically accelerated porous plate with slippage," European Journal of Mechanics - B/Fluids., vol. 72, pp. 135-143, 2018.

[12] M. Guria, "Unsteady MHD flow due to non-coaxial rotations of a porous disk and a fluid at infinity subjected to a periodic suction," International Journal of Applied Mechanics and Engineering., vol. 23, no. 3, pp. 623-633, 2018.

[13] A. Q. Mohamad, I. Khan, L. Y. Jiann, S. Shafie, Z. M. Isa and Z. Ismail, "Double convection of unsteady MHD non-coaxial rotation viscous fluid in a porous medium," Bulletin of the Malaysian Mathematical Sciences Society., vol. 41, no. 4, pp. 2117-2139, 2018.

[14] A. Q. Mohamad, Z. Ismail, N. F. M. Omar, M. Qassim, M. N. Zakaria, S. Shafie and L. Y. Jiann, "Exact solutions on mixed convection flow of accelerated non-coaxial rotation of MHD viscous fluid with porosity effect," Defect and Diffusion Forum., vol. 399, pp. 26-37, 2020.

[15] W. N. N. Noranuar, A. Q. Mohamad, S. Shafie and I. Khan, "Accelerated non-coaxial rotating flow of MHD viscous fluid with heat and mass transfer," IOP Conference Series: Materials Science and Engineering., vol. 1051, no. 1, pp. 012044, 2021.

[16] S. Rana, M. Z. Iqbal, M. Nawaz, H. Z. I. Khan, J. Alebraheem and A. Elmoasry, "Influence of chemical reaction on heat and mass transfer in MHD radiative flow due to non-coaxial rotations of disk and fluid at infinity," Theoretical Foundations of Chemical Engineering., vol. 54, no. 4, pp. 664-674, 2020.

[17]   M. Sheikholeslami, H. R. Ashorynejad, D. D. Ganji and A. Kolahdooz, "Investigation of rotating MHD viscous flow and heat transfer between stretching and porous surfaces using analytical method," Mathematical Problems in Engineering., vol. 11, no. 258734, pp. 1-17, 2011.

[18]   J. K. Singh and C. T. Srinivasa, "Unsteady natural convection flow of a rotating fluid past an exponential accelerated vertical plate with Hall current, ion-slip and magnetic effect," Multidiscipline Modeling in Materials and Structures., vol. 14, no. 2, pp. 216-235, 2018.

[19]   M. V. Krishna, "Hall and ion slip impacts on unsteady MHD free convective rotating flow of Jeffreys fluid with ramped wall temperature," International Communications in Heat and Mass Transfer., vol. 119, no. 104927, pp. 1-13, 2020.

[20]   A. J. Chamkha, A. S. Dogonchi and D. D. Ganji, "Magneto-hydrodynamic flow and heat transfer of a hybrid nanofluid in a rotating system among two surfaces in the presence of thermal radiation and Joule heating," AIP Advances., vol. 9, no. 2, pp. 1-15, 2019.

[21]   J. A. Gbadeyan, E. O. Titiloye and A. T. Adeosun, "Effect of variable thermal conductivity and viscosity on Casson nanofluid flow with convective heating and velocity slip," Heliyon., vol. 6, no. 1, pp. e03076, 2020.

[22]   M. Aneja, A. Chandra and S. Sharma, "Natural convection in a partially heated porous cavity to Casson fluid," International Communications in Heat and Mass Transfer., vol. 114, pp. 104555, 2020.

[23]   J. Venkatesan, D. S. Sankar, K. Hemalatha and Y. Yatim, "Mathematical analysis of Casson fluid model for blood rheology in stenosed narrow arteries," Journal of Applied Mathematics., vol. 2013, pp. 1-11, 2013.

[24]   C. Sulochana, G. P. Ashwinkumar and N. Sandeep, "Effect of frictional heating on mixed convection flow of chemically reacting radiative Casson nanofluid over an inclined porous plate," Alexandria Engineering Journal., vol. 57, no. 4, pp. 2573-2584, 2018.

[25]   N. Mahato, S. M. Banerjee, R. N. Jana and S. Das, "MoS2-SiO2/EG hybrid nanofluid transport in a rotating channel under the influence of a strong magnetic dipole (Hall effect)," Multidiscipline Modeling in Materials and Structures., vol. 16, no. 6, pp. 1595-1616, 2020.

[26]   N. Acharya, K. Das and P. K. Kundu, "Influence of multiple slips and chemical reaction on radiative MHD Williamson nanofluid flow in porous medium," Multidiscipline Modeling in Materials and Structures., vol. 15, no. 3, pp. 630-658, 2019.

[27]   N. A. M. Zin, I. Khan, S. Shafie and A. S. Alshomrani, "Analysis of heat transfer for unsteady MHD free convection flow of rotating Jeffrey nanofluid saturated in a porous medium," Results in Physics., vol. 7, pp. 288-309, 2017.

[28]   S. Dinarvand and I. Pop, "Free-convective flow of copper/water nanofluid about a rotating down-pointing cone using Tiwari-Das nanofluid scheme," Advanced Powder Technology., no. 28, vol. 3, pp. 900-909, 2017.

[29]   S. Das, B. Tarafdar and R. N. Jana, "Hall effects on magnetohydrodynamics flow of nanofluids due to non-coaxial rotation of a porous disk and a fluid at infinity," Journal of Nanofluids., vol. 7, no. 6, pp. 1172-1186, 2018.

[30]   T. S. Ashlin and B. Mahanthesh, "Exact solution of non-coaxial rotating and non-linear convective flow of Cu–Al2O3–H2O hybrid nanofluids over an infinite vertical plate subjected to heat source and radiative heat," Journal of Nanofluids., vol. 8, no. 4, pp. 781-794, 2019.

[31]   T. Tayebi, A. J. Chamkha and M. Djezzar, "Natural convection of CNT-water nanofluid in an annular space between confocal elliptic cylinders with constant heat flux on inner wall," Scientia Iranica B., vol. 26, no. 5, pp. 2770-2783, 2019.

[32]   N. Acharya, K. Das and P. K. Kundu, "Rotating flow of carbon nanotube over a stretching surface in the presence of magnetic field: a comparative study," Applied Nanoscience., vol. 8, no. 3, pp. 369-378, 2018.

[33]   B. Mahanthesh, B. J. Gireesha, I. L. Animasaun, T. Muhammad and N. S. Shashikumar, "MHD flow of SWCNT and MWCNT nanoliquids past a rotating stretchable disk with thermal and exponential space dependent heat source," Physica Scripta., vol. 94, no. 8, pp. 085214, 2019.

[34]   Z. Shah, E. Bonyah, S. Islam and T. Gul, "Impact of thermal radiation on electrical MHD rotating flow of Carbon nanotubes over a stretching sheet," AIP Advances., vol. 9, no. 015115, pp. 1-13, 2019.

[35]   P. Kumam, Z. Shahir, A. Dawar, H. U. Rasheed and S. Islam, "Entropy generation in MHD Radiative flow of CNTs Casson nanofluid in rotating channels with heat source/sink," Mathematical Problems in Engineering., vol. 2019, no. 9158093, pp. 1-14, 2019.

[36]   H. Saleh, A. Elham and A. Ebaid, "Medical applications for the flow of carbon-nanotubes suspended nanofluids in the presence of convective condition using Laplace transform," Journal of the Association of Arab Universities for Basic and Applied Sciences., vol. 24, no. 1, pp. 206-212, 2018.

[37]   A. Khalid, I. Khan, A. Khan, S. Shafie and I. Tlili, "Case study of MHD blood flow in a porous medium with CNTS and thermal analysis," Case Studies in Thermal Engineering., vol. 12, pp. 374-380, 2018.

[38]   A. Dawar, Z. Shah, S. Islam, M. Idress and W. Khan, "Magnetohydrodynamic CNTs Casson nanofluid and radiative heat transfer in a rotating channels," Journal of Physics Research and Applications., vol. 1, pp. 17-32, 2018.

[39]   Q. Z. Xue, "Model for thermal conductivity of carbon nanotube-based composites," Physica B: Condensed Matter., vol. 368, no. 11-4, pp. 302-307, 2005.

[40]   H. Villinger, "Solving cylindrical geothermal problems using the Gaver-Stehfest inverse Laplace transform," Geophysics., vol. 50, no. 10, pp. 1581-1587, 1985.

[41]   H. Stehfest, "Algorithm 368: Numerical inversion of Laplace transforms [D5]," Communications of the ACM., vol. 13, no. 1, pp. 47-49, 1970.